Powder Technology 225 (2012) 27–31

Contents lists available at SciVerse ScienceDirect

Powder Technology

journal homepage: www.elsevier.com/locate/powtec

Short communication

Structural characterization of mechanically milled and annealed tungsten powder

A.S. Bolokang [a], M.J. Phasha [b,*], Kasonde Maweja [c], S. Bhero [a]

[a] Department of Engineering Metallurgy, University of Johannesburg, P.O. Box 17011, Doornfontein 2028, South Africa
[b] Council for Scientific and Industrial Research (CSIR), Materials Science and Manufacturing, Meiring Naude, Brummeria, P.O. Box 395, Pretoria 0001, South Africa
[c] Element Six Ltd/Diamond Research Laboratory, P.O. Box 561, Springs 1559, Gauteng, South Africa

ARTICLE INFO

Article history:
Received 17 August 2011
Received in revised form 19 December 2011
Accepted 25 March 2012
Available online 30 March 2012

Keywords:
Nanocrystalline
Tungsten
Mechanical milling
Magnetic saturation

ABSTRACT

Nanocrystalline W powders with an average crystallite size of about 50 nm were produced by mechanical milling. BCT phase was mechanically induced as a result of BCC lattice deformation (compression) along [110], upon 10 h, 20 h and 30 h milling corresponding to a magnetic saturation of 1.3, 6.9, and 9.8 $\mu Tm^3/kg$. This BCT phase suggests the tetragonal deformation path to be responsible for the observed anomalous magnetism in W. Following DSC–TG thermal analysis, a magnetic saturation of 68 $\mu Tm^3/kg$ was obtained upon annealing the 30 h milled W powder at 1200 °C. In addition, two BCT phases with $c/a = 1.313$ ($a = 0.29066$, $c = 0.38170$ nm) and 0.907 ($a = 0.32602$, $c = 0.29575$ nm) were detected.

1. Introduction

In recent years, nanocrystalline (nc, grains sized below 100 nm) metals have captured a great attention due to their improved chemical, physical and mechanical properties compared with that of ultrafine crystalline (ufc, grain sizes ranging from 100 to 500 nm) or microcrystalline (mc, grains sized above 500 nm) metals. For ufc and mc metals, strength is drastically enhanced when grain size is reduced, following the Hall–Petch relationship [1,2]. Here, the pile-up of dislocations at grain boundaries is envisioned as the key mechanistic process underlying an enhanced resistance to plastic flow from grain refinement; when grain size is relatively large, greater stresses can be concentrated near adjacent grains due to multiple dislocation pile-ups, leading to the decrease in yield stress. On the other hand, as grain size is further reduced into nc region, activities of lattice dislocation become less significant, providing yield stress deviating from the Hall–Petch relationship [3–5].

Tungsten (W) is a useful body-centered-cubic (BCC) refractory metal. The W melting temperature of 3410 °C makes it suitable for high temperature applications such as filament of electric bulbs and substrate for polycrystalline diamond sintering. Its excellent mechanical strength, high density (19.3 g cm^{-3}), and sound velocity make it a potential material for kinetic energy ballistic penetrator [6,7]. These properties could be improved when fine-grained; nanocrystalline or amorphous W is produced [8–11]. In addition, W is a superconductor in a metastable beta (β) A15 phase when synthesized through reduction by hydrogen [12,13], inert-gas condensation [14], deposition [15,16], sputtering [17] and irradiation [18]. Several processing techniques for synthesis of nanocrystalline W powder include chemical routes such as sol–gel [19], combustion reactions [20] and mechanical milling (MM) [21,22]. MM has attracted considerable scientific interest in the last two decades due to its cost effectiveness and simplicity. It is an effective, versatile and economic tool for preparation of nanocrystalline powders. MM process has become a state-of-the-art processing technique recently used to synthesize composite, equilibrium and non-equilibrium (amorphous, quasicrystals, nanocrystalline, etc.) materials that are of commercial and scientifically interest [23–29]. This powder metallurgy process involves repeated cold welding and fracturing of powder particles subjected to high-energy by impacting balls which causes fracture and sometimes plastic deformation. Although nanocrystalline W powder has being produced via MM before [21,22], the reports on lattice deformation which leads to phase transformation due to MM of W powder are scarce [30]. It is well known that in the production of nanocrystalline size powders of pure metals, phase transformation can be induced [31,32]. The phase transformation depends on the crystalline size and lattice strain induced by mechanical energy [32]. The objective of the current study is to investigate the effect of MM on production of nanocrystalline W powder and possible deformation path, which induces anomalous magnetism reported recently [30]. In addition, we study the thermal stability of milled W powder as well as the annealing effect on the deformed crystal structure and magnetism.

2. Experimental work

The starting material consisted of tungsten powder (99.5% purity) supplied by Boart Longyear (South Africa) with particle size distribution

* Corresponding author. Tel.: +27 12 841 3196; fax: +27 12 841 3378.
E-mail address: mphasha@csir.co.za (M.J. Phasha).

0032-5910/$ – see front matter © 2012 Elsevier B.V. All rights reserved.
doi:10.1016/j.powtec.2012.03.028

parameters $d_{10} = 2$ μm, $d_{50} = 5$ μm and $d_{90} = 8$ μm. Ball milling of W powder was conducted in a high energy ball mill at 650 rpm and 20:1 ball-to-powder ratio for duration of 10, 20 and 30 h. In order to minimize contamination due to interstitial elements, no process control agent (PCA) was added during milling. The changes in morphology of powder were analyzed using the LEO 1525 field-emission scanning electron microscope (FE-SEM) coupled with a Robinson backscatter electron detector (RBSD) and an Oxford Link Pentafet energy dispersive X-ray spectroscopy (EDX) detector. Crystal structure evolution was traced with a PANalytical X'Pert PRO PW 3040/60 X-ray diffractometer equipped with a Cu K_α ($\lambda = 0.154$ nm) monochromated radiation source and 0.02° step size scanned from 20 to 90° (2θ). The Microtac Bluewave particle analyzer was employed to determine the particle size of unmilled and milled W powders.

Thermal analysis was carried out using DSC and TG incorporated in NETZSCH STA. The powder samples were heated up to 1200 °C and cooled to room temperature with Al_2O_3 as a baseline at a heating rate of 20 °C/min under argon atmosphere.

Magnetic saturation of the milled powders was determined using a commercial saturation induction measuring system (LDJ Electronics Inc.). The system was calibrated using pure cobalt and pure nickel references. The test piece of the milled powder was weighed and inserted into a non-magnetic holder. It was introduced into a permanent magnet (~0.75 T), and then was quickly withdrawn. The response of a search coil was displayed on a magnetic multimeter in terms of magnetic moment (saturation). Each measurement was repeated to check consistency of results. Following the DSC–TG thermal analysis, which indicated transformation temperature, the powder milled for 30 h was annealed at 1100 and 1200 °C in a tube furnace under inert atmosphere.

3. Results and discussions

3.1. Powder characterization

Fig. 1(a) through to (d) shows the SEM morphology of W powder milled for 0, 10, 20, and 30 h. The unmilled powder is comprised of fine network of nest-like particles with diameters 2.89, 5.42 and 8.14 μm for cumulative d_{10}, d_{50} and d_{90}, as shown in Table 1. Upon 10 h and 20 h milling, very fine (below 2 μm) and big lump (around 12 μm) particles became evident as shown in Fig. 1(b). The d_{10} and d_{50} reduced in size while coarser particle d_{90} increased after 10 h and 20 h of milling. The formation of large particles is attributed to cold welding, whereas fine particles are a result of fracturing. After 30 h, the d_{90} became larger than 104 μm.

Fig. 2 represents X-ray diffraction patterns of W powders milled and annealed. As shown in Fig. 2(a), the BCC W is revealed by its primary XRD peaks of (110), (002), (211) and (220) planes [33]. A new peak emerged on the shoulder of (110) plane upon milling for 10 h and beyond. The shoulder peak is attributed to the deformation of BCC lattice when compressed along [110] to form a body-centered-tetragonal (BCT) structure labeled 1' with lattice parameters $a = 0.31451$ and $c = 0.32052$ nm in accordance with the established Bain's transformation path for deformation of iron (Fe) [34–36], hence the shift of (110) peak towards higher angles, as detected by the XRD. After 10 h milling, it is evident that the XRD peak intensity increased abruptly due to preferred crystal orientation, as was observed in the case of milling titanium [37], and slightly reduced on further milling to 20 h and 30 h although still higher than those of the unmilled. The peaks became broader after milling due to crystal refinement [38–40] as evidenced by calculated crystallite sizes labeled D_S and D_{WH} in Fig. 3(a) and (b) using both Scherrer equation [37–39] and Williamson–Hall (W–H) methods [40], respectively.

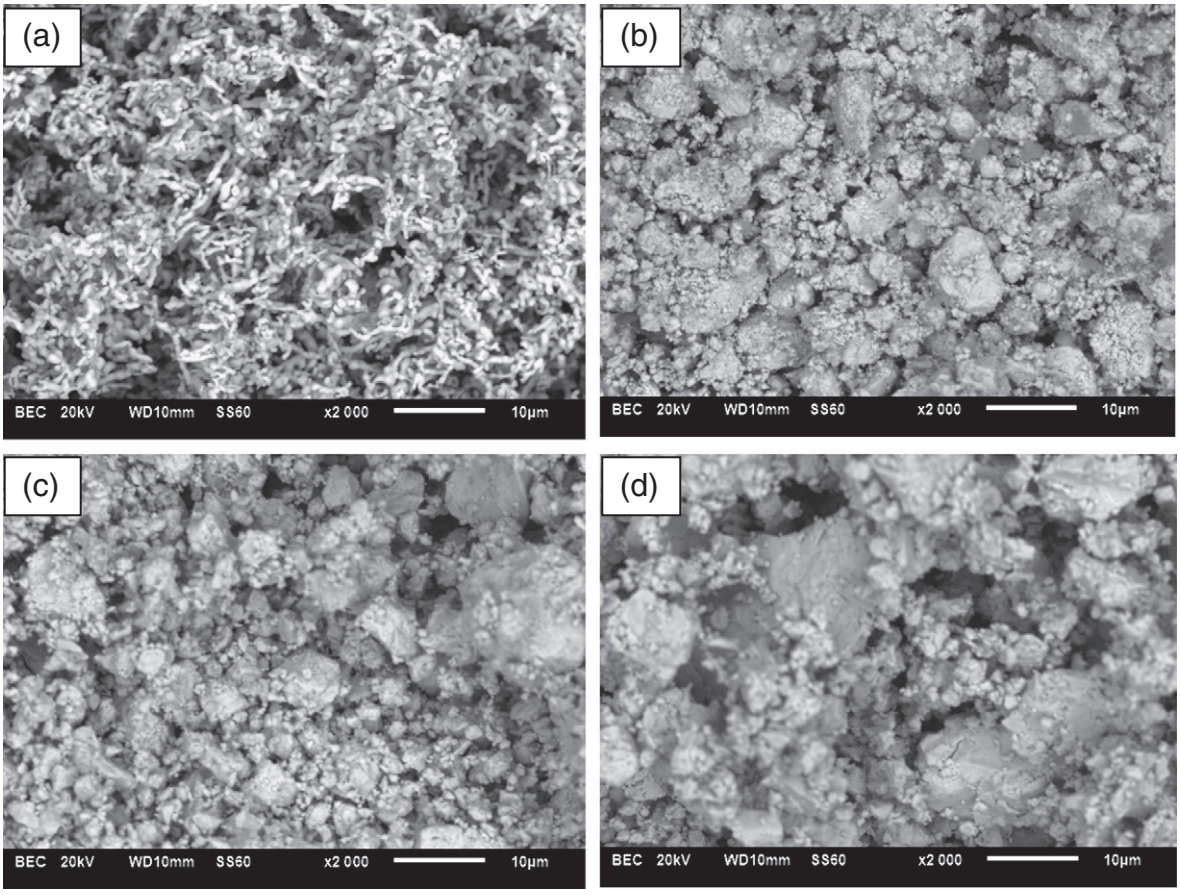

Fig. 1. SEM micrograph of (a) unmilled, (b) 10 h, (c) 20 h and (d) 30 h ball milled W powders.

Table 1
Particle size distribution as a function of milling time.

Milling time (h)	D_{10} (μm)	D_{50} (μm)	D_{90} (μm)
0	2.89	5.42	8.14
10	1.51	4.39	12.33
20	1.49	4.83	11.95
30	1.51	6.94	104.90

Fig. 3(a) shows a decrease in average crystallite size (D_S) of unmilled W (304 nm) to 34, 50 and 31 nm after 10 h, 20 h and 30 h of milling, respectively, calculated by the Scherrer method. Similar trend of crystallite size against milling time was observed when using the W–H method, although the determined crystallite size was smaller for unmilled powder, equal after 10 h, and slightly larger for 20 h and 30 h in comparison to those obtained using Scherrer equation. The increase in crystalline size after 20 h (50 nm) could be due to cold welding of particles. The corresponding microstrain vs. milling time curve indicates that the crystals became highly strained after 20 h and 30 h, yielding 0.27 and 0.42 percent strain, respectively.

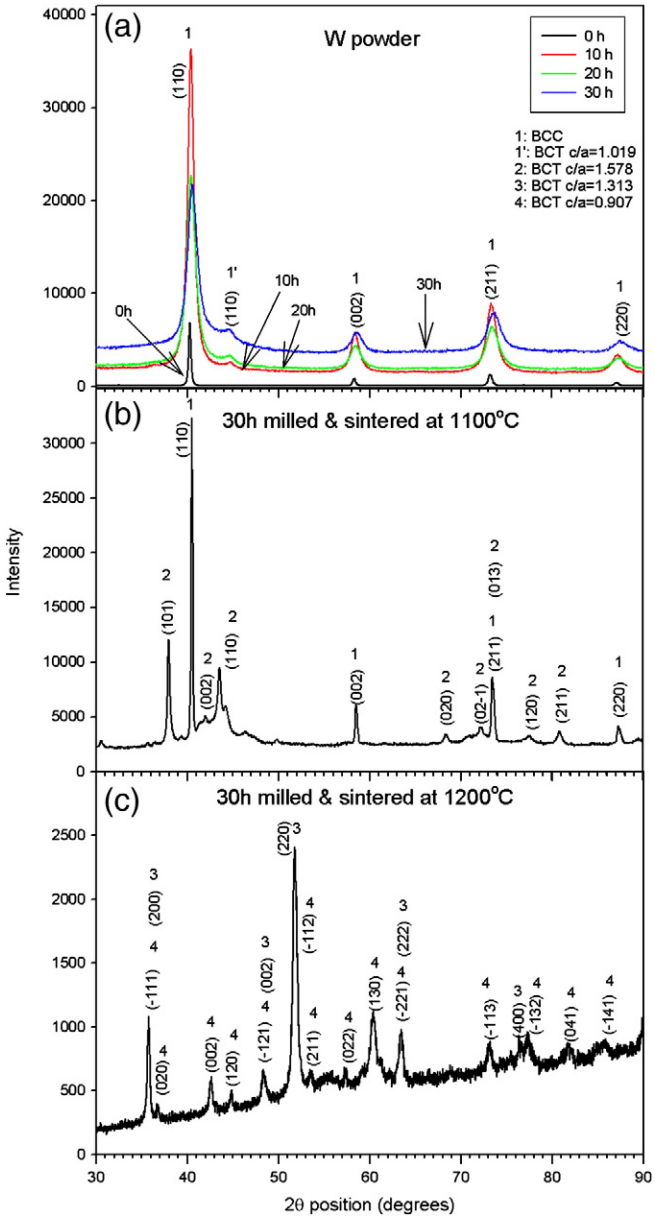

Fig. 2. XRD patterns of W (a) milled for 0, 10, 20, 30 h, (b) milled for 30 h and annealed at 1100 °C and (c) annealed at 1200 °C.

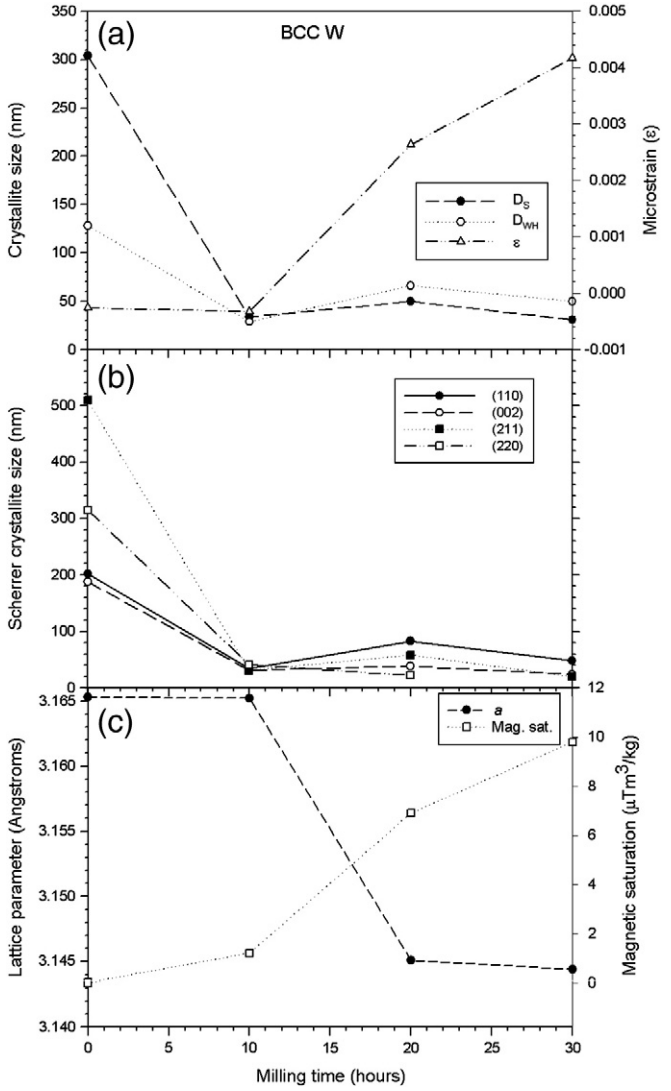

Fig. 3. (a) Average Scherrer, W–H crystalline sizes and microstrain, (b) Scherrer crystallite size determined on (110), (002), (211), and (220) planes and (c) lattice parameter and magnetic saturation, as a function of milling time.

Fig. 3(b) shows the determined Scherrer crystalline sizes on (110), (002), (211) and (220) individual planes. In general, the established trends are similar to the average, more especially for (110) and (211) planes since crystallite sizes along (002) and (220) planes become constant on further milling beyond 10 h.

The lattice parameter of W (0.31650 nm) was not significantly altered by milling for 10 h as shown in Fig. 3(c), while 20 h and 30 h milling induced a pronounced lattice deformation as evidenced by reduction to 0.31451 and 0.31444 nm, respectively. In addition, a non-magnetic W powder displayed an increase in magnetic saturation with progressive milling as shown in Fig. 3(c). The magnetic saturation has increased from 0 to 1.3, 6.9, and 9.8 $\mu Tm^3/kg$ after 10 h, 20 h and 30 h, respectively. The observed increase in magnetic saturation reaching a maximum of about 15 $\mu Tm^3/kg$ after 24 h was recently reported when milling was conducted at lower speed of 350 rpm [30]. Hence, further studies on the effect of milling kinetics on inducing magnetism of pure W are necessary to establish the genesis for this anomalous magnetic behavior. Theoretically, it has been articulated that the presence or absence of magnetism in transition metals is determined by a competition between intra-

atomic exchange interactions and inter-atomic electron motion [41]. Since the inter-atomic motion depends strongly on the inter-atomic separation, and because the *d* bands are partially filled, transition metals are necessarily magnetic at sufficiently large volumes (low density) and necessarily nonmagnetic at sufficiently low volumes (high densities) [41–45]. Thus, a normally magnetic transition metal, like iron, becomes nonmagnetic when compressed. Conversely, a normally nonmagnetic transition metal, like tungsten, becomes magnetic when expanded [41–45]. However, the nature of the transition from nonmagnetic to magnetic behavior constitutes a long-standing problem [41].

3.2. Thermal stability of W powders

Fig. 4 shows the DSC and TG curves of W powder milled for 0, 10 h, 20 h and 30 h heat treated from room temperature to 1200 °C. The DSC curve of unmilled W powder represented by "0" shows a smooth and broad exothermic peak, which could be attributed to a relief of strain induced by cold compaction of powder, followed by sudden endothermic behavior just above 1000 °C. The corresponding TG curve indicates mass loss with minimum at about 250 °C, after which mass gain is observed until 1200 °C. The DSC curve for 10 h milled powder is almost similar to that of unmilled powder although shallow and distinct endothermic peaks are observed at 800 and 1072 °C, respectively. These two endothermic peaks correspond to respective mass losses as a result of volume expansion, as shown by TG curves. Correlation of endothermic peak and mass loss could be attributed to second-order magnetic transition as evidenced by increased magnetic saturation to 68 $\mu Tm^3/kg$ upon annealing the 30 h milled W powder at 1200 °C. Similar thermal behavior was previously observed in milled nickel powder, which conversely resulted in reduced Curie temperature [46]. This hypothesis became clear upon milling for 20 h and 30 h, in which shallow endothermic peak became more pronounced and the corresponding mass losses became sharp. In addition, another endothermic peak, which does not correspond to any mass loss, is observed at 1189 °C. Therefore, the peak at 1189 °C corresponds to first-order phase transformation while at 1072 °C corresponds to magnetic transition. Upon annealing at 1100 °C, BCC and BCT phases with lattice parameters $a = 0.31560$ and $a = 0.27341$, $c = 0.43147$ nm, respectively, were detected as shown in Fig. 2(b). Furthermore, the lattice parameters *a* and *c* of the BCT phase with $c/a = 1.578$ are similar to those of HCP Os (Reference pattern code 01-087-0716 in ICDD PDF2 database within the PANalytical X'Pert High Score software), as was recently reported in Ref. [30]. According to Bain deformation path [39–41] (see Supplementary data), the BCT with $c/a = 1.578$ implies an FCT phase beyond FCC phase, since at FCC the c/a of BCT phase is equal to $\sqrt{2}$.

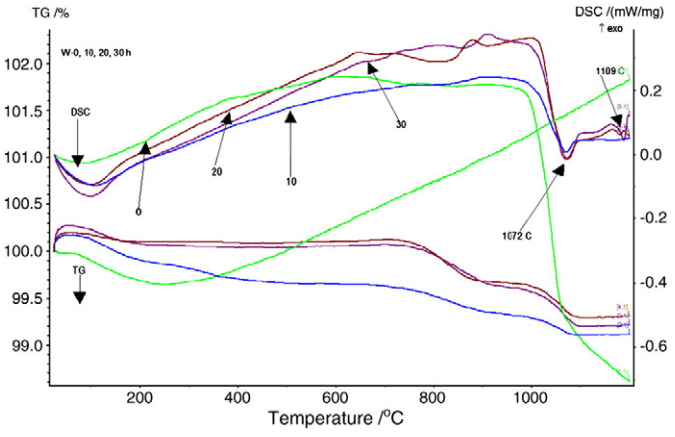

Fig. 4. DSC–TG curves for 0, 10, 20 and 30 h milled W powder.

The above method assumes constant unit cell volume of $V = a^2c$ during tetragonal deformation. As shown in Fig. 2(c), two BCT phases with $c/a = 1.313$ ($a = 0.29066$, $c = 0.38170$ nm) and 0.907 ($a = 0.32602$, $c = 0.29575$ nm) were obtained after annealing at 1200 °C. It therefore follows from these XRD results that the endothermic peak at 1189 °C corresponds to the transformation from BCT with $c/a > \sqrt{2}$ to BCT with $c/a < \sqrt{2}$, hence the peak correlates to unstable FCC lattice when $c/a = \sqrt{2}$ (for clarity, see supporting theoretical results as well as Refs. [34–36] which show maximum energy at this point).

4. Conclusion

Nanocrystalline W powders with an average crystallite size of about 50 nm were produced by MM. BCT phase was mechanically induced as result of BCC lattice deformation (compression) along [110], upon 10 h, 20 h and 30 h milling corresponding to magnetic saturation of 1.3, 6.9, and 9.8 $\mu Tm^3/kg$. This BCT phase suggests the tetragonal deformation path to be responsible for the observed anomalous magnetism in W. Following DSC–TG thermal analysis, a magnetic saturation $\mu_s = 68\ \mu Tm^3/kg$ was obtained upon annealing at 1200 °C the powder milled for 30 h. In addition, two BCT phases with $c/a = 1.313$ ($a = 0.29066$, $c = 0.38170$ nm) and 0.907 ($a = 0.32602$, $c = 0.29575$ nm) were detected.

Supplementary data to this article can be found online at doi:10.1016/j.powtec.2012.03.028.

References

[1] E.O. Hall, The deformation and ageing of mild steel: III Discussion of results, Proceedings of the Physical Society. Section B 64 (1951) 747–753.
[2] N.J. Petch, The cleavage strength of polycrystals, Journal of the Iron and Steel Institute 174 (1953) 25–28.
[3] V. Yamakov, D. Wolf, S.R. Phillpot, H. Gleiter, Grain-boundary diffusion creep in nanocrystalline palladium by molecular-dynamics simulation, Acta Materialia 50 (2002) 61–73.
[4] H. Gleiter, Nanostructured materials: basic concepts and microstructure, Acta Materialia 48 (2000) 1–29.
[5] H. Gleiter, Nanostructured materials: state of the art and perspectives, Nanostructured Materials 6 (1995) 3–14.
[6] Q. Wei, K.T. Ramesh, B.E. Schuster, L.J. Kecskes, R.J. Dowding, Nanoengineering opens a new era for tungsten as well, Journal of Metals 58 (2006) 40–44.
[7] S. Pappu, S. Sen, L.E. Murr, D. Kapoor, L.S. Magness, Deformation twins in oriented, columnar-grained tungsten rod ballistic penetrators, Materials Science and Engineering A 298 (2001) 144–157.
[8] O. El-Atwani, D.V. Quach, M. Efe, P.R. Cantwell, B. Heim, B. Schultz, E.A. Stach, J.R. Groza, J.P. Allain, Multimodal grain size distribution and high hardness in fine grained tungsten fabricated by spark plasma sintering, Materials Science and Engineering A 528 (2011) 5670–5677.
[9] L. Magness, L. Kecskes, M. Chung, D. Kapoor, F. Biancianello, S. Ridder, Behaviour and performance of amorphous and nanocrystalline metals in ballistic impacts, 19th International Symposium of Ballistic, 7–11 May (2001), Interlaken, Switzerland, 2001, pp. 1183–1189.
[10] K. Cho, L. Kecskes, R. Dowding, B. Schuster, Q. Wei, R.Z. Valiev, Nanocrystalline and ultrafine grained tungsten for kinetic energy penetrator and warhead linear applications, Proceedings of the 25th Army Science Conference, Orlando, FL, 27 November (2006), 2006.
[11] B.R. Klotz, F.R. Kellorgg, E.M. Klier, R.J. Dowding, K.C. Cho, Characterization, Processing, and Consolidation of Nanoscale Tungsten Powder, Army Research Laboratory, Aberdeen Proving Ground, MD, 21005–5069, 2009, pp. 1–24.
[12] W.R. Morcom, W.L. Worrell, H. Sell, H.I. Kaplan, The preparation and characterization of beta-tungsten, a metastable tungsten phase, Metallurgical Transactions 5 (1974) 155–161.
[13] H. Huimin, C. Xinmin, Metastable characteristics of β-W, Acta Metallurgica Sinica 2 (1989) 184–188.
[14] W. Krauss, R. Birringer, Metastable phases synthesized by inert-gas-condensation, Nanostructured Materials 9 (1997) 109–112.
[15] T. Krabacak, P.-I. Wang, G.-C. Wang, T.-M. Lu, Phase transformation of single crystal β-tungsten nanorods at elevetated temperatures, Thin Solid Films 493 (2005) 293–296.
[16] J.P. Singh, T. Karabacak, T.-M. Lu, G.-C. Wang, Nanoridge domains in α-phase W films, Surface Science Letters 538 (2003) 483–487.
[17] H.L. Sun, Z.X. Song, D.G. Guo, F. Ma, K.W. Xu, Microstructure and mechanical properties of nanocrystalline tungsten thin films, Journal of Materials Science and Technology 26 (2010) 87–92.
[18] C.L. Chen, T. Nagase, H. Mori, In situ TEM observations of irradiation-induced phase change in tungsten, Journal of Materials Science 44 (2009) 1965–1968.

[19] Y. Han, T. Qiu, T. Song, Preparation of ultrafine tungsten powder by sol–gel method, Journal of Materials Science and Technology 24 (2008) 816–818.
[20] H.H. Nersisyan, H.I. Won, C.H. Won, K.C. Cho, Combustion synthesis of nanostructured tungsten and its morphological study, Powder Technology 189 (2009) 422–425.
[21] E. Oda, H. Fujiwara, K. Ameyama, Nano grain formation in tungsten by severe plastic deformation-mechanical milling process, Materials Transactions 49 (2008) 54–57.
[22] Q.V. Tolochko, O.G. Klimova, S.S. Ordanian, D.-I. Cheong, Y.M. Kim, Effects of tungsten nanoparticles additions on the densification of micron size tungsten powder, Reviews on Advanced Materials Science 21 (2009) 192–199.
[23] E. Ma, Alloys created between immiscible elements, Progress in Materials Science 50 (2005) 413–509.
[24] M.S. El-Eskandarany, Mechanical Alloying for Fabrication of Advanced Engineering Materials, William Andrew Publishing, Norwich, New York, USA, 2001.
[25] R.W. Gardiner, P.S. Goodwin, S.B. Dodd, B.W. Viney, Non-equilibrium synthesis of new materials, Advanced Performance Materials 3 (1996) 343–364.
[26] M.J. Phasha, K. Maweja, C. Babst, Mechanical alloying by ball milling of Ti and Mg elemental powders: operation condition considerations, Journal of Alloys and Compounds 492 (2010) 201–207.
[27] K. Maweja, L.A. Cornish, N. Can, Transformation and alloying mechanisms in sub-stoichiometric titanium carbonitrides-tungsten high energy ball milled powders, International Journal of Refractory Metals and Hard Materials 29 (2011) 312–319.
[28] K. Maweja, L.A. Cornish, N. Can, Formation mechanism of nanocrystalline tungsten–titanium aluminides by ball milling of Ti(C, N)–W powders at subzero temperature, Powder Technology 211 (2011) 221–225.
[29] K. Maweja, M. Phasha, N. van der Berg, Microstructure and crystal structure of an equimolar Mg–Ti alloy processed by Simoloyer high-energy ball mill, Powder Technology 199 (2010) 256–263.
[30] K. Maweja, M.J. Phasha, L.J. Choenyane, Thermal stability and magnetic saturation of annealed nickel-tungsten and tungsten milled powders, International Journal of Refractory Metals and Hard Materials 30 (2012) 78–84.
[31] I. Manna, P.P. Chattopadhyay, P. Nanadi, F. Banhart, H.J. Fecht, Formation of face-centered-cubic titanium by mechanical attrition, Journal of Applied Physics 93 (2003) 1520–1524.
[32] M.J. Phasha, A.S. Bolokang, P.E. Ngoepe, Solid-state transformation in nanocrystalline Ti induced by ball milling, Materials Letters 64 (2010) 1215–1218.
[33] ICSD Database FIZ Karlsruhe 2009–02, version 2.3.
[34] L.G. Wang, M. Šob, Z. Zhang, Instability of higher-energy phases in simple and transition metals, Journal of Physics and Chemistry of Solids 64 (2003) 863–872.
[35] M. Šob, L.G. Wang, V. Vitek, Local stability of higher-energy phases in metallic materials and its relation to the structure of extended defects, Computational Materials Science 8 (1997) 100–106.
[36] P.J. Craievich, M. Weinert, J.M. Sanchez, R.E. Watson, Local stability of none-quilibrium phases, Physical Review Letters 72 (1994) 3076–3079.
[37] A.S. Bolokang, M.J. Phasha, Formation of titanium nitride produced from nanocrystalline titanium powder under nitrogen atmosphere, International Journal of Refractory Metals and Hard Materials 28 (2010) 610–615.
[38] B.E. Warren, X-ray Diffraction, Addison-Wesley Publishing, Massachusetts, 1969.
[39] J.I. Langford, A.J.C. Wilson, Scherrer after sixty years: a survey and some new results in the determination of crystallite size, Journal of Applied Crystallography 11 (1978) 102–113.
[40] G.K. Williamson, W.H. Hall, X-ray line broadening from filed aluminium and wolfram, Acta Metallurgica 1 (1953) 22–31.
[41] V.L. Moruzzi, Singular volume dependence of transition-metal magnetism, Physical Review Letters 57 (1986) 2211–2214.
[42] V.L. Moruzzi, P.M. Marcus, Magnetism in bcc 3*d* transition metals: onset and approach to the Hund's-rule limit, Physical Review B 38 (1988) 1613–1620.
[43] T.M. Hattox, J.B. Conklin Jr., J.C. Slater, S.B. Trickey, Calculation of the magnetization and total energy of vanadium as a function of lattice parameter, Journal of Physics and Chemistry of Solids 34 (1973) 1627–1638.
[44] D. Stoeffler, H. Dreyssé, Strong or weak ferromagnetism in transition metals, Solid State Communications 79 (1991) 645–649.
[45] J.L. Fry, Y.Z. Zhao, N.E. Brener, G. Fuster, J. Callaway, Prediction of ferromagnetism in bcc Mn, Physical Review B 36 (1987) 868–871.
[46] A.S. Bolokang, M.J. Phasha, Thermal analysis on the curie temperature of nanocrystalline Ni produced by ball milling, Advanced Powder Technology 22 (2011) 518–521.